Electronic Supplementary Material (ESI) for Chemical Communications.

Supplementary information

An efficient method to prepare supported bismuth nanoparticles as highly selective electrocatalyst for the conversion of CO_2 into formate

Matteo Miola, Bart C. A. de Jong and Paolo P. Pescarmona

Chemical Engineering Group, Engineering and Technology Institute Groningen, University of Groningen, Nijenborgh 4, 9747 AG Groningen, the Netherlands. E-mail: *p.p.pescarmona@rug.nl*

Content

Reagents 2

Synthesis 2

Literature overview 2

Physicochemical characterisation 5

Ink and electrode preparation 8

Electrochemical characterisation 8

Products characterisation 10

Post-catalysis characterisation 13

Bismuth loading effect 14

Reference electrocatalyst prepared by electrodeposition method 15

References 15

Reagents

Bismuth(III) subsalicylate 99.9% (BiSub), ethanol 96%, dimethyl sulphoxide 99.9% (DMSO), sodium bicarbonate > 99.7% ($NaHCO_3$), deuterium oxide 99.8% (D_2O), bismuth (III) nitrate, nitric acid 70% and Nafion 117 (5 wt%) were purchased from Sigma Aldrich. Norit SX1G activated carbon (AC) was purchased from Cabot.

Synthesis

In a 50 mL round-bottom flask, 0.5090 g of activated carbon were mixed with 0.5852 g of bismuth(III) subsalicylate and 25 mL of ethanol. After stirring overnight (8 h), the slurry was dried via rotaevaporation and dried overnight (8 h) at 90 °C in an oven. The obtained material was labelled BiSub@AC. The dried powder was pyrolysed under N_2 atmosphere (flow: 100 mL min^{-1}) at 400 °C for 1 h (ramp: 25 °C min^{-1}) in a tubular oven. The obtained material was labelled BiSub@AC-400.

Literature overview

Table S1: Literature overview on Bi-based electrocatalysts for the CO_2-to-formate conversion.

Catalyst	E (V_{RHE})[a]	η (V)[b]	FE_{HCOO^-}[c]	$\lvert j_{HCOO^-} \rvert$ (mA cm^{-2})[d]	γ_{HCOO^-} (A g^{-1})[e]	$\gamma_{Bi,\ HCOO^-}$ (A g^{-1})[f]	t_{LTE} (h)[g]	Area (cm^2)[h]	Ref.
$Bi_2O_2CO_3$ NS (4 nm thick) [l]	−0.70	0.50	85%	9.4	9.4	11.4	12	1	[1]
µm Bi^0 dendrites [m]	−0.73	0.53	89%	2.4	2.2	–	12	–	[2]
S-Bi µm needles [l]	−0.75	0.55	84%	4.3	10.1	12.4	24	1.5	[3]
Bi^0 clusters (µm) [m]	−0.78	0.58	87%	1.3	0.4	0.4	20	4	[4]
BOC NS (20−40 nm thick) [i]	−0.79	0.59	83%	0.83	0.6	0.73	27	0.2	[5]
Bi_2O_3 NF (250 ± 50 nm) [i]	−0.80	0.60	90%	3.6	2.1	2.1	10	–	[6]
Bi NS (10 nm thick) [l]	−0.80	0.60	94%	4.6	5	6.15	12	1	[7]
Bi NS (10 nm thick) [l]	−0.83	0.63	95%	15.3	10.2	25.8	10	1	[8]
Bi NTs (Ø~100 nm) [m]	−0.85	0.65	> 99%	42.0	42.0	46.8	48	1	[9]
Bi/BiO_x µm dendrites [i]	−0.86	0.66	91%	2.7	6.6	6.6	4	1	[10]
Bi NPs@N-CP (20 nm) [i]	−0.87	0.67	92%	13.2	58.4	114.3	24	–	[11]
Bi NS-NGQDs [m]	−0.87	0.67	98%	16.5	7.1	9.5	15	1	[12]
Bi NPs@C (10 nm) [m]	−0.87	0.67	> 99%	4	4.44	22.2	4	–	[13]
Bi_2O_3 flakes (µm) [i]	−0.90	0.70	84%	9.1	4.9	5.5	2	0.2	[14]
BiOBr NFs [i]	−0.90	0.70	95%	52.8	0.47	1	65	4	[15]
Bi_2O_3 NS (200 nm) [m]	−0.90	0.70	91%	7.3	7.3	8.1	24	0.2	[16]
Bi cluster (100 nm) [m]	−0.93	0.73	98%	9.7	12.9	17.2	14	0.07	[17]
Bi_2O_3@Bi NPs (20 nm) [m]	−0.97	0.77	95%	5.1	51.0	158	32	1	[18]
Bi_2O_3 NS@N-CP [m]	−1.00	0.8	94%	14.1	0.2	0.2	24	3	[19]
BiSub@AC-400 [l]	**−1.07**	**0.87**	**> 99%**	**6.2**	**16**	**34**	**24**	**1.3**	**This work**
BiO_x NS (10 nm thick) [m]	−1.16	0.96	95%	54.1	81.6	101.7	–	0.07	[20]

[a] Potential (E) rounded to the tens of mV, at which the maximum Faradaic efficiency (FE) towards formate was obtained. [b] Overpotentials (η) calculated using $E^0(CO_2/HCOO^-)$ = −0.2 V_{RHE} and rounded to the tens of mV. [c] FE_{HCOO^-} at the reported conditions. [d] Fraction of the current density leading to formate (over geometric electrode area) at the reported potential. [e] Mass activity (γ_{HCOO^-}) defined as the fraction of current leading to formate over the specific electrocatalyst mass load on the electrode. [f] Mass activity ($\gamma_{Bi,\ HCOO^-}$) defined as the fraction of current leading to formate over the specific bismuth mass load on the electrode, if not specified in the respective publication its values has been calculated. [g] Maximum bulk electrolysis time (t_{LTE}) reported for stability studies. [h] Electrode geometric area. Experiment performed with [i] 0.1 M $KHCO_3$, [l] 0.5 M $NaHCO_3$ or [m] 0.5 M $KHCO_3$ electrolyte. NS, NF, NT and NP stands as abbreviations for nanosheets, nanoflakes, nanotubes and nanoparticles, respectively.

Table S2: Literature overview on Bi-based electrocatalysts synthesis procedures.

Ref.	Bi source/ Precursor/support method/	Synthesis steps
[1]	Bi NS/ $Bi_2O_2CO_3$/ el. exfoliation	1) El. exfoliation: E = 10 V, d = 1.5 cm 2) Centrifugation 3) Cleaning
[2]	$Bi(NO_3)_3 \cdot 5H_2O$/ Bi film on Cu/ el. red.	1) 100 nm e-beam evap. Bi on Cu 2) El. reduction: E = -1.8 V vs Ag/AgCl, 60 s, 10÷30x 3) Cleaning
[3]	$Bi(NO_3)_3 \cdot 5H_2O$/ hydrothermal/ Bi_2S_3	1) Autoclave: 200 °C, 24 h 2) Centrifugation 3) Washing 4) Vacuum drying
[4]	$Bi(NO_3)_3 \cdot 5H_2O$/ chem. red./ GDE	1) N_2H_4 reduction: 100 °C, 1 h, N_2 2) Centrifugation 3) Washing 4) Drying: 75 °C, 6 h
[5]	$Bi(NO_3)_3 \cdot 5H_2O$/ $Bi_2O_2CO_3$/ el. red.	1) 90 °C 4h 2) Centrifugation 3) Washing 4) Drying: 60 °C, 12 h 5) El. reduction: E = -1.5 V vs Ag/AgCl, 1 h
[6]	$Bi(NO_3)_3 \cdot 5H_2O$/ el. red./ Cu film	1) Pulsed el. red. E = -0.1 V vs. Ag/AgCl ($\sim$ 40 mA cm^{-2}), 6 cycles 2) Cleaning
[7]	$Bi(NO_3)_3 \cdot 5H_2O$/ $Bi_2O_2CO_3$ NS/ hydrothermal, el. red.	1) Autoclave: 150 °C, 12 h, in NMP 2) Washing 3) Lyophilisation 4) El. reduction: E = -0.62 V vs Ag/AgCl, 2 h
[8]	$Bi(NO_3)_3 \cdot 5H_2O$/ BiOI/ hydrothermal, el. red.	1) Autoclave: 160 °C, 2 h, KI 2) Washing 3) Lyophilisation 4) El. reduction: E = -1.55 V vs Ag/AgCl, 2 h
[9]	$Bi(CH_3COO)_3$/ chemical red. / Bi_2O_3 NTs/ calcination	1) 195 °C, 15 min, N_2 2) Washing 3) Centrifugation 4) Lyophilisation 5) Calcination: 300 °C, 1 h, air
[10]	$Bi(NO_3)_3 \cdot 5H_2O$/ el. red./ Cu plate	1) El. reduction: E = -1.0 V vs Ag/AgCl, 25 min, 65 °C on Cu 2) Cleaning
[11]	$Bi(NO_3)_3 \cdot 5H_2O$/ chem. red. /N-CP	1) ZIF-67 treated at 800 °C, 3 h, Ar, HNO_3 at 80 °C, 3 h 2) Impregnation and $NaBH_4$ reduction 3) Centrifugation, washing 4) Drying: 60 °C
[12]	$Bi(NO_3)_3 \cdot 5H_2O$/ hydrothermal/ Bi_2O_3 on NGQDs	1) Autoclave: 160 °C, 5 h with NGQDs (4 nm) 2) Centrifugation 3) Washing 4) Vacuum drying: 60 °C, 12 h
[13]	$BiCl_3$/ chem. red./ CP	1) $NaBH_4$ reduction in DMF with carbon powder 2) Filtering 3) Cleaning 4) Drying

[14]	$Bi(NO_3)_3 \cdot 5H_2O$/ hydrothermal/ Bi_2O_3/ el. red.	1) Autoclave: 130 °C, 6 h 2) Calcination: 500 °C, 2 h 3) El. reduction: E = -1.5 V vs Ag/AgCl, 5 min
[15]	$BiBr_3$/ chemical red./ BiOBr	1) Dissolution in DMSO (glovebox, N_2) 2) Deposition on GDE (140°C)
[16]	$NaBiO_3 \cdot 2H_2O$/ chemical red. / Bi_2O_3 /calcination	1) 200 °C, 24 h 2) Centrifugation 3) Washing 4) Vacuum drying: 70 °C, 12 h 5) Calcination: 200 °C, 5 h, air
[17]	$Bi(NO_3)_3 \cdot 5H_2O$/ $BiOCl_{0.5}Br_{0.5}$/ chemical red.	1) 140 °C, 24 h with KCl and KBr 2) Filtration 3) Washing 4) Drying: 80 °C, 12 h
[18]	$Bi(NO_3)_3 \cdot 5H_2O$/ Bi(btb) MOF/ hydrothermal	1) Autoclave: 120 °C, 12 h 2) Washing 3) Activation: 160 °C, 12 h
[19]	$Bi(NO_3)_3 \cdot 5H_2O$/ N-CP/ hydrothermal	1) Autoclave: 160 °C, 6 h with N doped CP 2) Washing 3) Drying: 80 °C
[20]	$BiCl_3$/ BiOCl/ chemical, el. red.	1) Precipitation: -10 °C 1h 2) Aging: 12 h 3) Washing 4) Vacuum drying 5) El. reduction: E = -0.2 V to -1.4 V vs RHE, 3 cycles

The electrochemical reduction of the electrocatalysts during the electrochemical conversion of CO_2 to $HCOO^-$ is implied in the synthesis procedure and not reported in the table. The bismuth-based electrocatalysts for CO_2 to $HCOO^-$ electrochemical conversion can be produced by: (a) chemical reduction methods, which require the use of a reducing agent;[4, 9, 11, 13] (b) electrochemical reduction methods, which would need to be re-optimised for different electrode dimensions and cell configurations;[2, 5-8, 10, 14, 20] and (c) hydrothermal reduction methods, which need to be re-optimised when changing the scale of the autoclave setup.[3, 12, 18, 19] Furthermore, the need for multiple washing steps hinders the applicability of many of these methods on the large scale. CP stands for carbon paper and N-CP stands for nitrogen-doped CP.

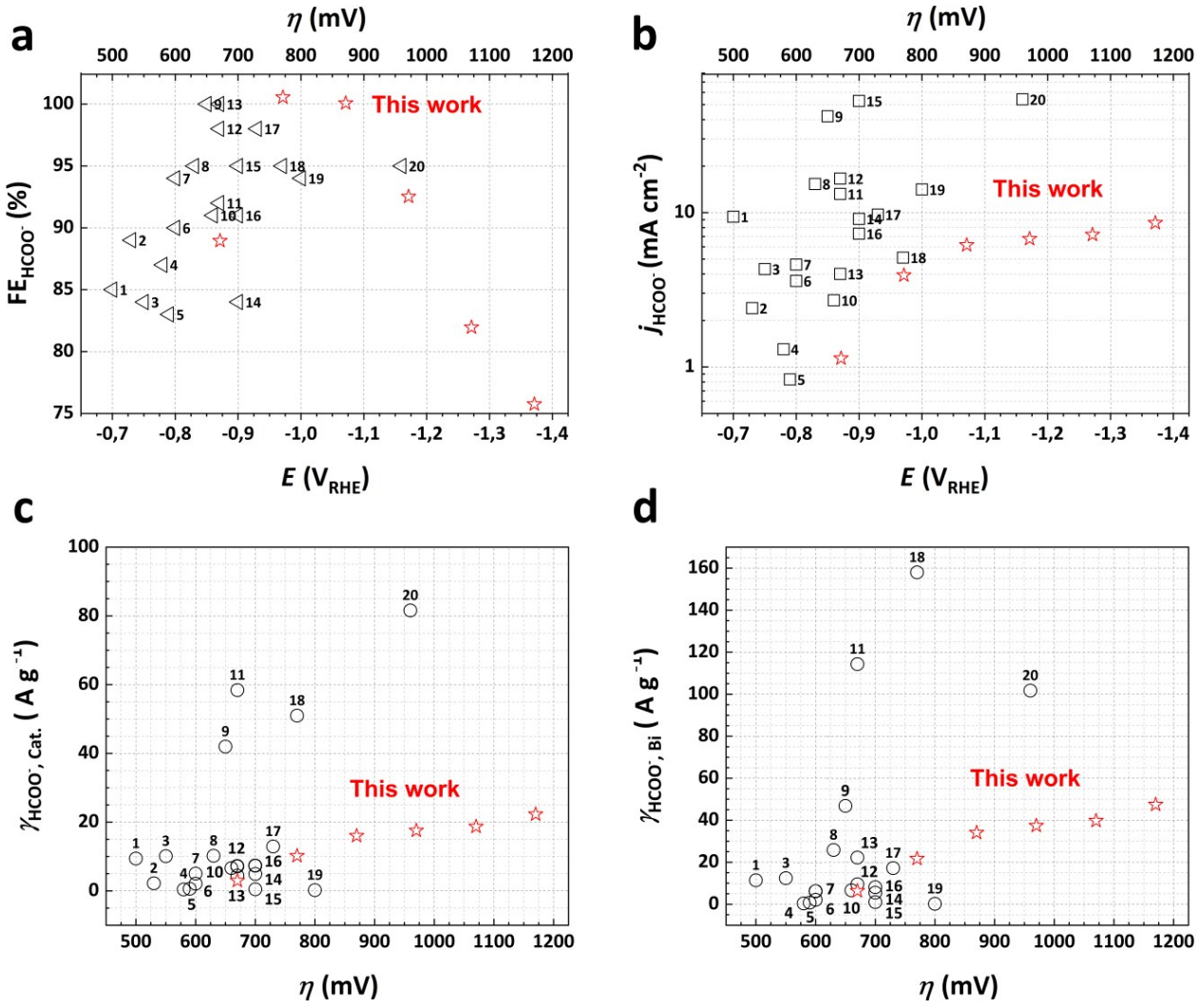

Figure S1: Literature overview of the performance of the Bi-based electrocatalysts for the CO_2-to-formate conversion in terms of: (a) Faradaic efficiency; (b) fraction of current density leading to formate; (c) mass activity; and (d) mass activity per bismuth content. The values for the BiSub@AC-400 catalyst are represented with red stars.

Physicochemical characterisation

X-ray diffraction (XRD) measurements were performed on a D8 Advance Bruker diffractometer with a Cu Kα1 radiation (λ = 1.5418 Å) under 40 kV and 40 mA in the range of 10-80°.

Nitrogen physisorption isotherms were measured at -196 °C using a Micromeritics ASAP 2420 apparatus. The specific surface area was estimated via the Brunauer-Emmet-Teller (BET) method.

Scanning transmission electron microscopy (STEM) was performed with a Fei ThemisZ equipment operating at 300 kV with a HAADF detector. The energy-dispersive X-ray spectroscopy (EDX) mapping was performed with a Bruker dual detector system (the analysing software is Velox version 2). The samples were prepared by grinding the solid material in a mortar with a pestle (opal white), followed by suspension of the fine powder in isopropyl alcohol and dropcast on a holey carbon grid. The TEM particle analysis was carried out on different pictures for a total of 90 different particles (Fig. S2). The average particle size was calculated to be 5.5 ± 2 nm (maximum of the lognormal distribution function and its FWHM/2), Fig. S3. The TEM images were processed with the use of ImageJ software.

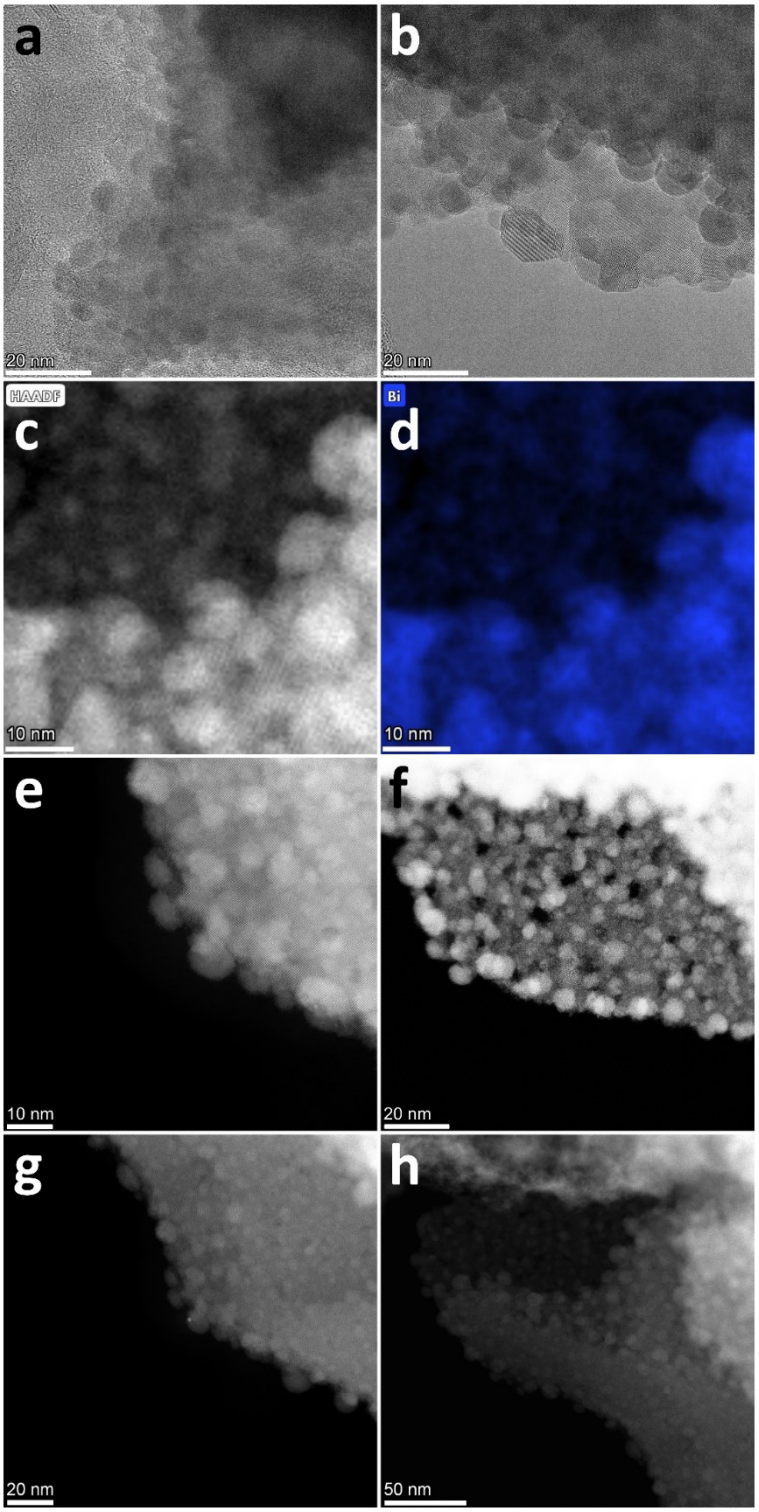

Figure S2: STEM pictures (a, b), HAADF TEM pictures (c, e, f, g, h) and EDX STEM picture (d) corresponding to the HAADF TEM picture (c).

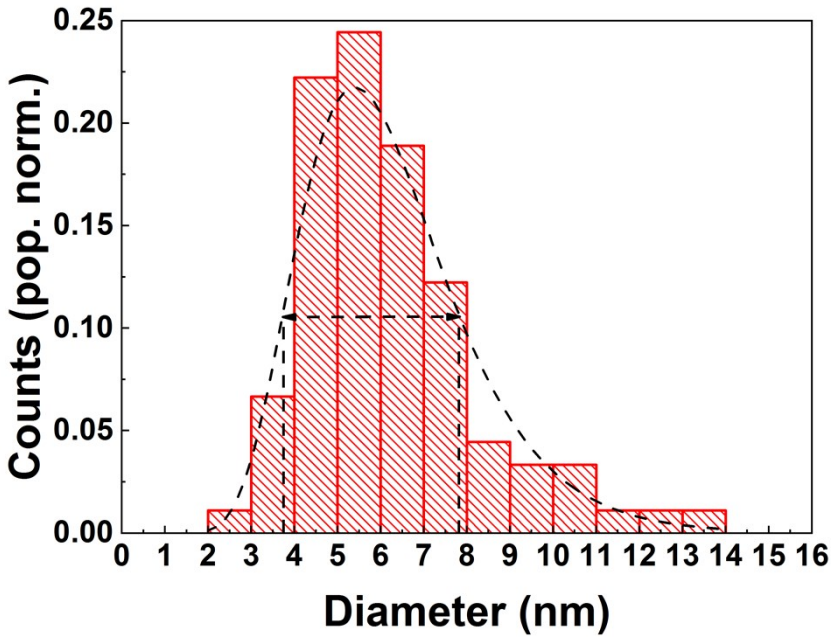

Figure S3: Histogram representing the distribution of the diameters of the bismuth nanoparticles.

Inductively coupled plasma optical emission spectrometry (ICP-OES) was performed on a Perkin Elmer Optima 7000 DV equipment. The samples were prepared suspending a weighted amount of material in 7 mL HNO_3. The suspension was treated in a microwave oven at 200 °C for 10 min (from room temperature to 200 °C in 10 min). The volume of sample was increased with concentrated aqueous HNO_3 up to 50 mL. After x10 dilution, the sample was centrifuged and measured. The Bi, C and H contents obtained from the analysis are reported in Table S3.

Table S3: ICP-OES elemental analysis.

Sample	Bi wt%	C wt%	H wt%
BiSub@AC-400	47.0 ± 0.1	42.2 ± 0.5	0.26 ± 0.01

Thermogravimetric analysis (TGA) was performed on a thermogravimetric analyser TGA4000 from Perkin Elmer under air or N_2 (flow: 21 ml min^{-1}) and with a temperature ramp of 5 °C min^{-1}.

The Bi wt% was calculated measuring the total weight loss in the TGA performed in air (Fig. S4). In oxygen rich atmosphere, the totality of the carbon phase is removed and the metallic bismuth (M_W = 208.98 g mol^{-1}) is expected to be fully oxidised to Bi_2O_3 (M_W = 465.96 g mol^{-1}). The Bi wt% calculated under these assumptions is reported in Table S4. The experimental values obtained for BiSub and BiSub@AC fit between 1% to the theoretical values. On the other hand, the 41.5 wt% calculated for BiSub@AC-400 is slightly lower compared to the bismuth content obtained via ICP-OES characterisation (47 wt%). This difference suggests that a fraction of the bismuth that is present in metallic form in BiSub@AC-400 does not get oxidised to Bi_2O_3 during the TGA analysis, with consequent underestimation of the bismuth content.

Table S4: Theoretical and experimental bismuth content (the latter being obtained via TGA analysis).

Material	Theoretical Bi wt%	Experimental Bi wt%
BiSub	57.7	57.0
BiSub@AC	30.9	32.0
BiSub@AC-400		41.5

In the TGA analysis in air of the BiSub and BiSub@AC (Fig. S4a), the mass loss between 125 and 200 °C can be attributed to the degradation of the subsalicylic acid ligand,[21] the mass loss at ca. 250 °C can be attributed to the degradation of the C-O-Bi coordination,[22] the mass losses at 300 °C and 400 °C are attributed to the carbon degradation catalysed by the Bi species.[23, 24] The mass loss at T > 700 °C is due to bismuth phase changes.[24]

In the TGA analysis under N_2 of the BiSub and BiSub@AC (Fig. S4b), despite the similar transition temperatures, the presence of activated carbon alters the degradation behaviour of BiSub for T > 340 °C, increasing the relative transition temperatures of 7 °C (T = 343 °C) and 23 °C (T = 388°C).

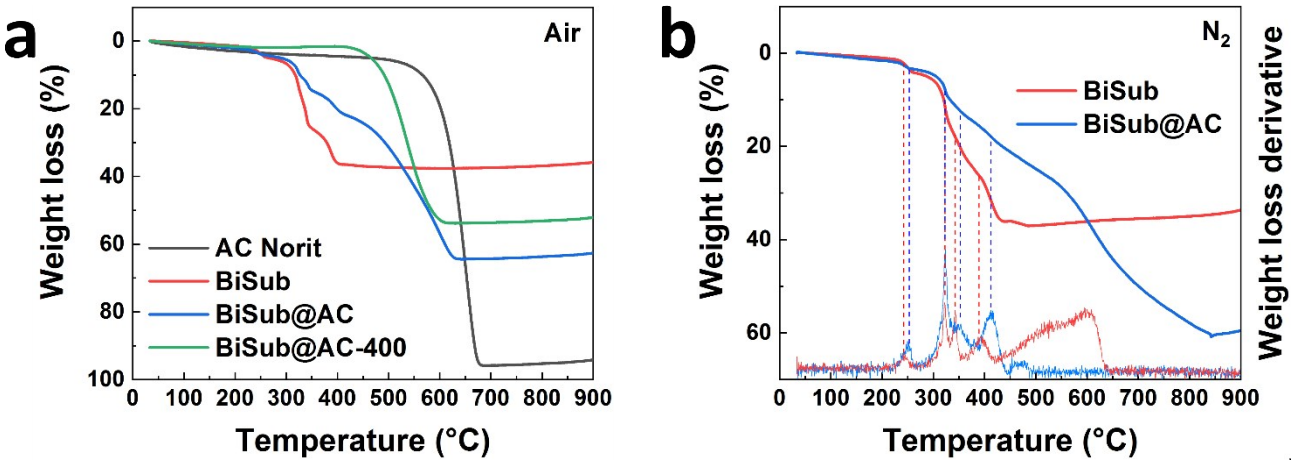

Figure S4: (a) TGA analysis of AC Norit, BiSub, BiSub@AC and BiSub@AC-400 in air; (b) TGA analysis of BiSub and BiSub@AC in N_2 and the relative weight loss derivatives.

Ink and electrode preparation

The working electrodes (WE) were prepared on glassy carbon (GC) plates (Sigradur G, HTW) polished with 1 µm diamond paste prior to utilisation. The glassy carbon plates were coated with adhesive Teflon tape leaving a square open surface of 1.3 cm^2. 12 mg of the BiSub@AC-400 electrocatalyst were mixed with 1080 µL of 96% ethanol and 120 µL of Nafion 117 (5 wt%). The slurry was mixed for 1 h in an ultrasound bath. After sonication, 50 µL of the suspension were drop-casted on the GC plates and allowed to dry in a fume hood for 2 h. The procedure results in a 0.385 mg cm^{-2} loading of BiSub@AC-400 on the GC plate.

Electrochemical characterisation

Cyclic voltammetry and controlled potential electrolyses were performed with an Autolab potentiostat with Nova software. In all the experiments, a 0.5 M $NaHCO_3$ aqueous electrolyte was used (7 mL for the catholyte and 7 mL for the anolyte), saturated with CO_2 for 10 min before each specific experiment. The H-cell was equipped with a GC plate as WE, a Pt mesh as counter electrode (CE) and a Ag/AgCl (3.5 M KCl) leak-free reference electrode (RE, Alvatek: LF-1-100). The two compartments were separated via a Nafion membrane. The controlled-potential electrolyses were performed with constant CO_2 bubbling (50 sccm) for 30 min. Upon CO_2 saturation, the electrolyte pH changed from pH = 8.4 to pH = 7.3. For the stability test electrolysis, an H-cell with a 36 mL cathodic and a 36 mL anodic compartment was used. The two electrochemical cells are presented in Fig. S5. The RHE scale was used to account for the pH change. The CO_2-to-$HCOO^-$ standard potential is -0.19 V vs RHE.[18]

$$E(V_{RHE}) = E(V_{Ag/AgCl}) + E^{0}_{Ag/AgCl}(V_{NHE}) + 0.059 \times pH \qquad E^{0}_{Ag/AgCl} = 0.198\, V_{NHE}$$

Current density: $j\ (mA\ cm^{-2})$, current: $i\ (mA)$, electrode geometric area: $A_{geom}\ (cm^{-2})$: $j = \frac{i}{A_{geom}}$

Mass activity: $\gamma\ (A\ g^{-1})$, current: $i\ (A)$, catalyst mass: $m_{cat}\ (g)$: $\gamma = \frac{i}{m_{cat}}$

Mass activity relative to the bismuth content: $\gamma_{Bi}\ (A\ g^{-1})$, current: $i\ (A)$, bismuth mass: $m_{Bi}\ (g)$: $\gamma_{Bi} = \frac{i}{m_{Bi}}$

The FE and *J* values and their associated errors in Fig. 4 were calculated as average and standard deviation from four distinct repeated experiments.

The electrochemical surface area (ECSA) of the AC support and of BiSub@AC-400 were estimated by measuring the capacitance (C) of the electrode in a 0.5 M $NaHCO_3$ aqueous solution saturated for 10 min with CO_2.

$ECSA = \frac{C}{C_{ref}}$ $\Delta i/2 = C \cdot \nu$ ν : scan rate

The capacitance values at 0.1 V and -0.4 V for AC and BiSub@AC-400 (Fig. S5c) were obtained based on the cyclic voltammograms performed at different scan rates (Fig. S5a and b). These results show that the capacitance of BiSub@AC-400, and thus its ECSA decreases of 54% compared to the corresponding values for AC ($ECSA_{BiSub@AC-400}/ECSA_{AC} = C_{BiSub@AC-400}/C_{AC} = 0.46$) to. The decrease is comparable with the decrease in surface area measured via gas sorption (N_2) of 54% (from 784 to 358 m^2/g).

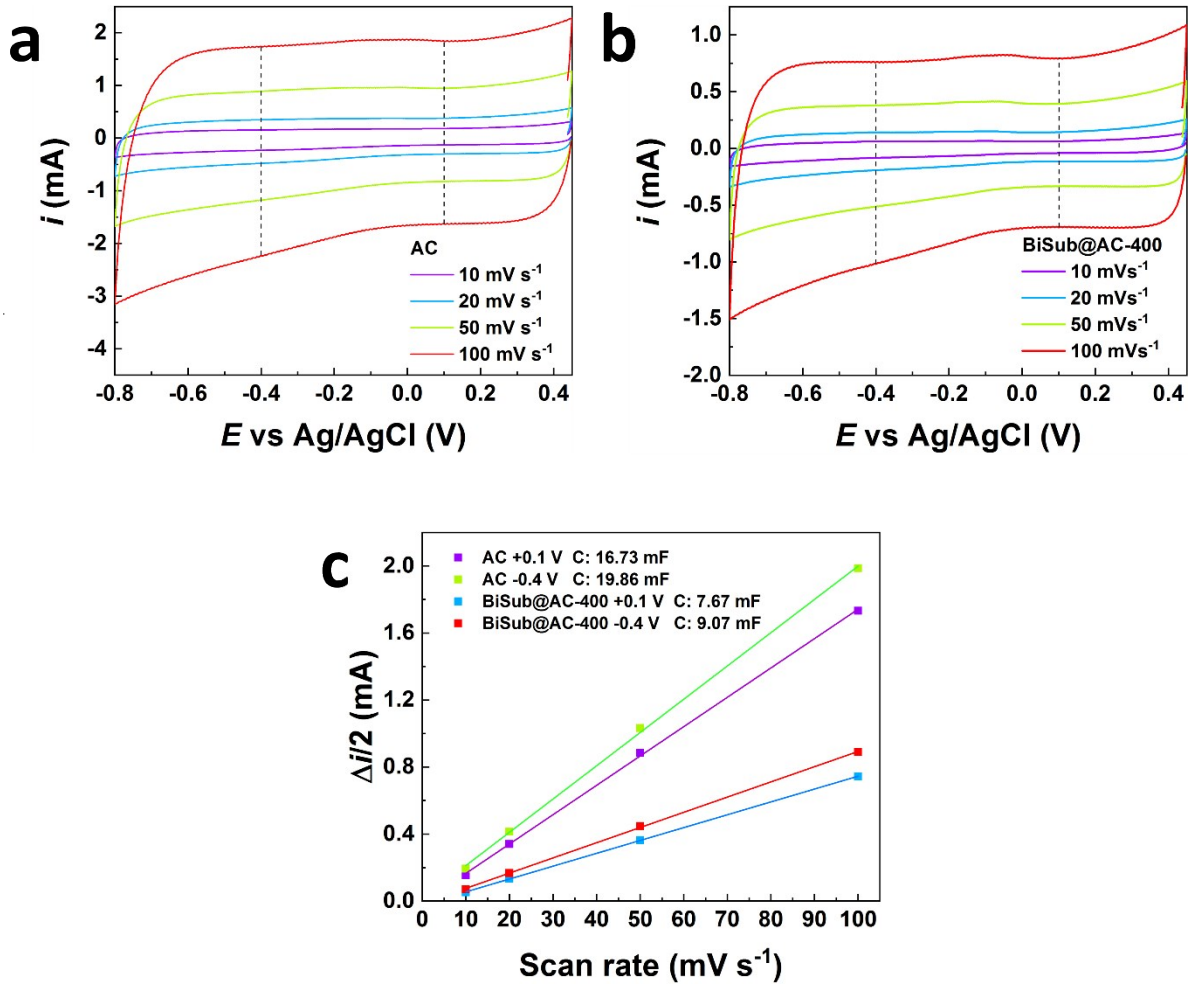

Figure S5: Cyclic voltammetry at 10, 20, 50 and 100 mV s^{-1} in CO_2-sat. 0.5 M $NaHCO_3$ of (a) AC and (b) BiSub@AC-400; (c) change in the double layer capacitive current density, Δi/2, recorded as a function of the scan rate, v, on AC and BiSub@AC-400 at different potentials (-0.4 V in green and red and +0.1 V in purple and blue).

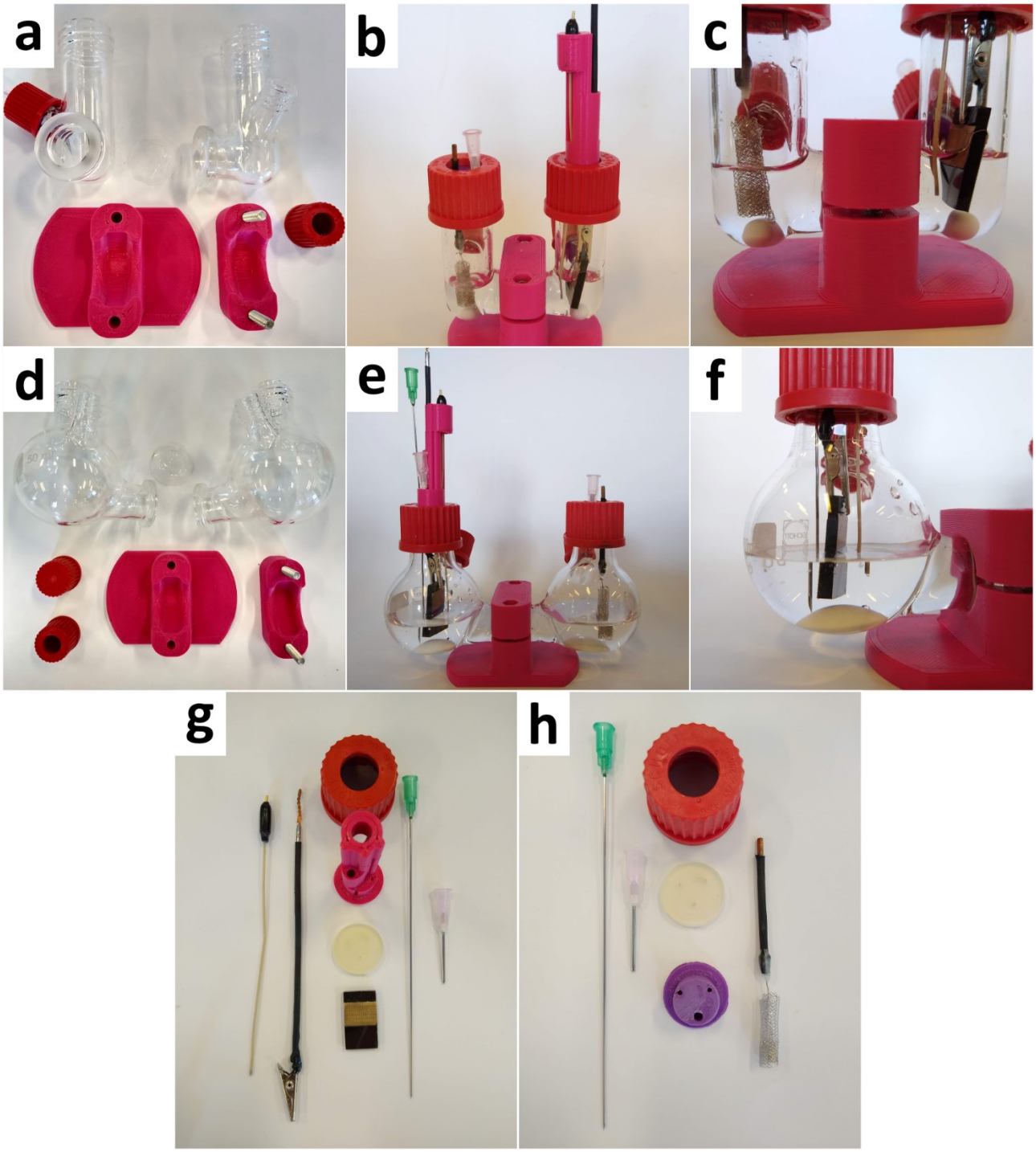

Figure S6: Pictures of the electrochemical H-cell, in the exploded version, assembled and with zoom on the cathodic compartment for the catholyte volume of V = 7 mL (a, b, c) and for the catholyte volume of V = 36 mL (d, e, f). Cathodic and anodic compartment components (g and h).

Products characterisation

The analysis of the liquid products was carried both via HPLC and ^{1}H-NMR. The HPLC analysis was carried with an Agilent Technologies 1200 series equipped with Bio-Rad Aminex HPX-87H 300 × 7.8 mm column at T = 60 °C with 0.5 mM aqueous H_2SO_4 eluent (flow rate: 0.55 mL min^{-1}) and a refractive index detector. The ^{1}H-NMR analysis was carried with a Bruker ascend 600 mHz spectrometer with water suppression method. The HPLC samples were prepared mixing 1 g of the electrolyte (after controlled potential electrolysis) and 0.5 g

of a standard aqueous solution containing DMSO (0.03 M) and $NaHCO_3$ (0.5 M). The NMR samples were prepared mixing 0.5 g of the electrolyte (after controlled potential electrolysis), 0.1 g of the standard solution of DMSO and $NaHCO_3$, and 0.1 g of D_2O.

The Faradaic efficiency (FE) was calculated via the following equation.

$$FE_{HCOO^-} = \frac{2 \times F \times n_{HCOO^-}}{Q} \times 100\%$$

Where 2 is the number of electrons involved in the reaction, F is the Faraday constant (96485.3 C mol^{-1}), Q is the charge measured during the test (C) and n_{HCOO^-} are the produced moles of formate (mol).

As an example, a typical HPLC chromatogram, the HPLC calibration curve, a representative ^{1}H-NMR spectrum and its calibration curve are shown in Fig. S6.

The detection of the gas products was carried out with an online compact GC (CGC) from Interscience, equipped with a paramond (CO_2, C_{2+}) and a molsieve (H_2, O_2, N_2, CO, CH_4) column.

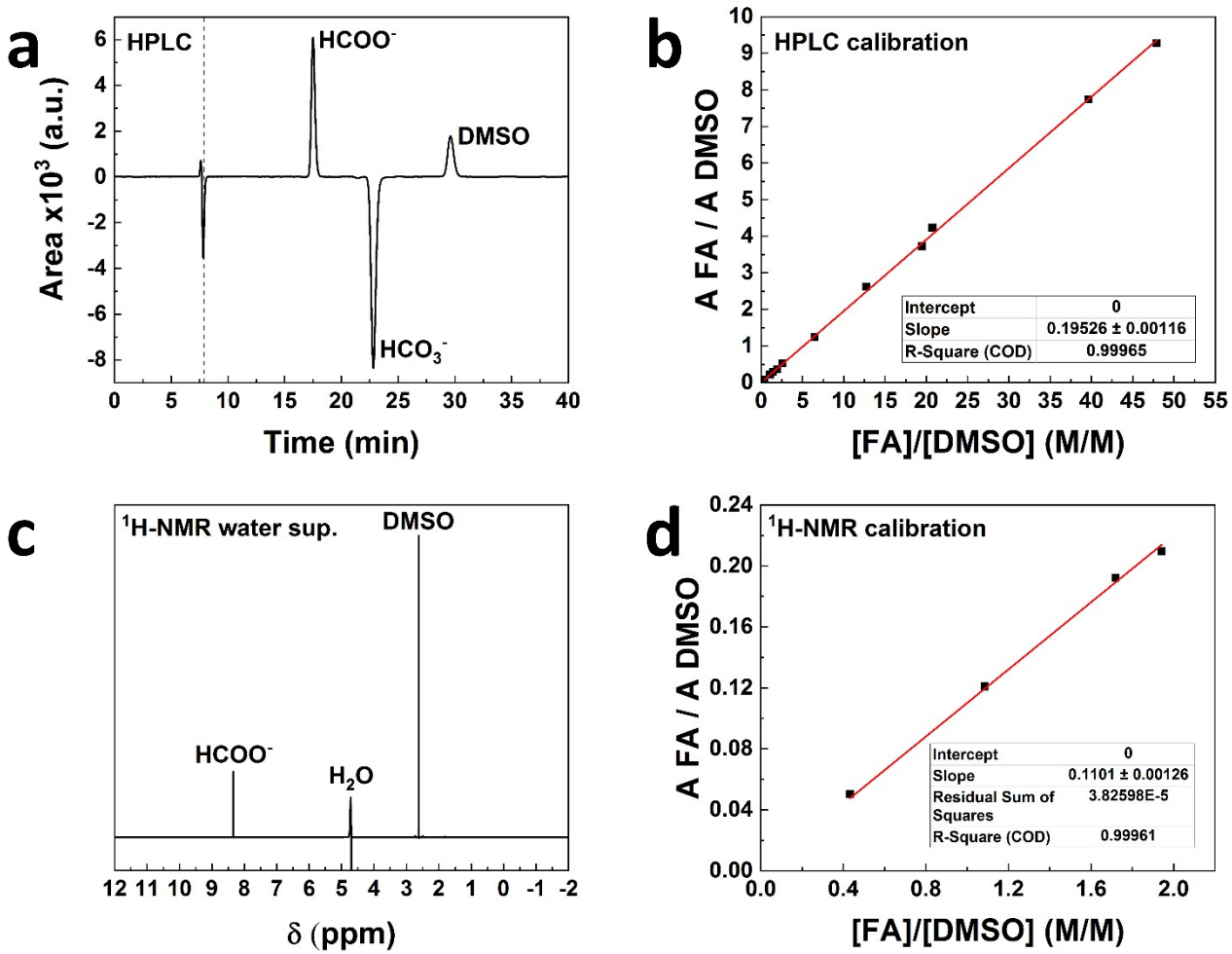

Figure S7: Representative HPLC chromatogram (a) and ^{1}H-NMR spectrum (b), and respective calibration curves (c, d).

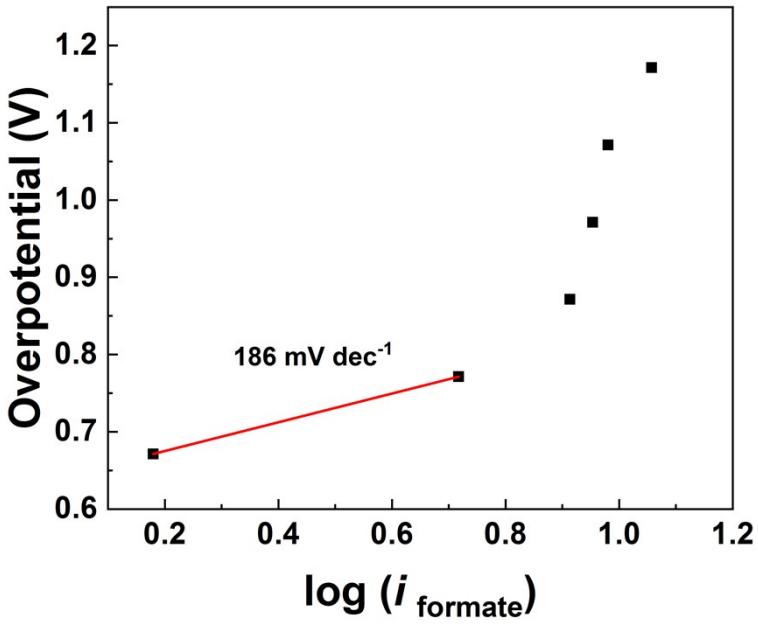

Figure S8: Tafel plot for formate production over BiSub@AC-400.

Post-catalysis characterisation

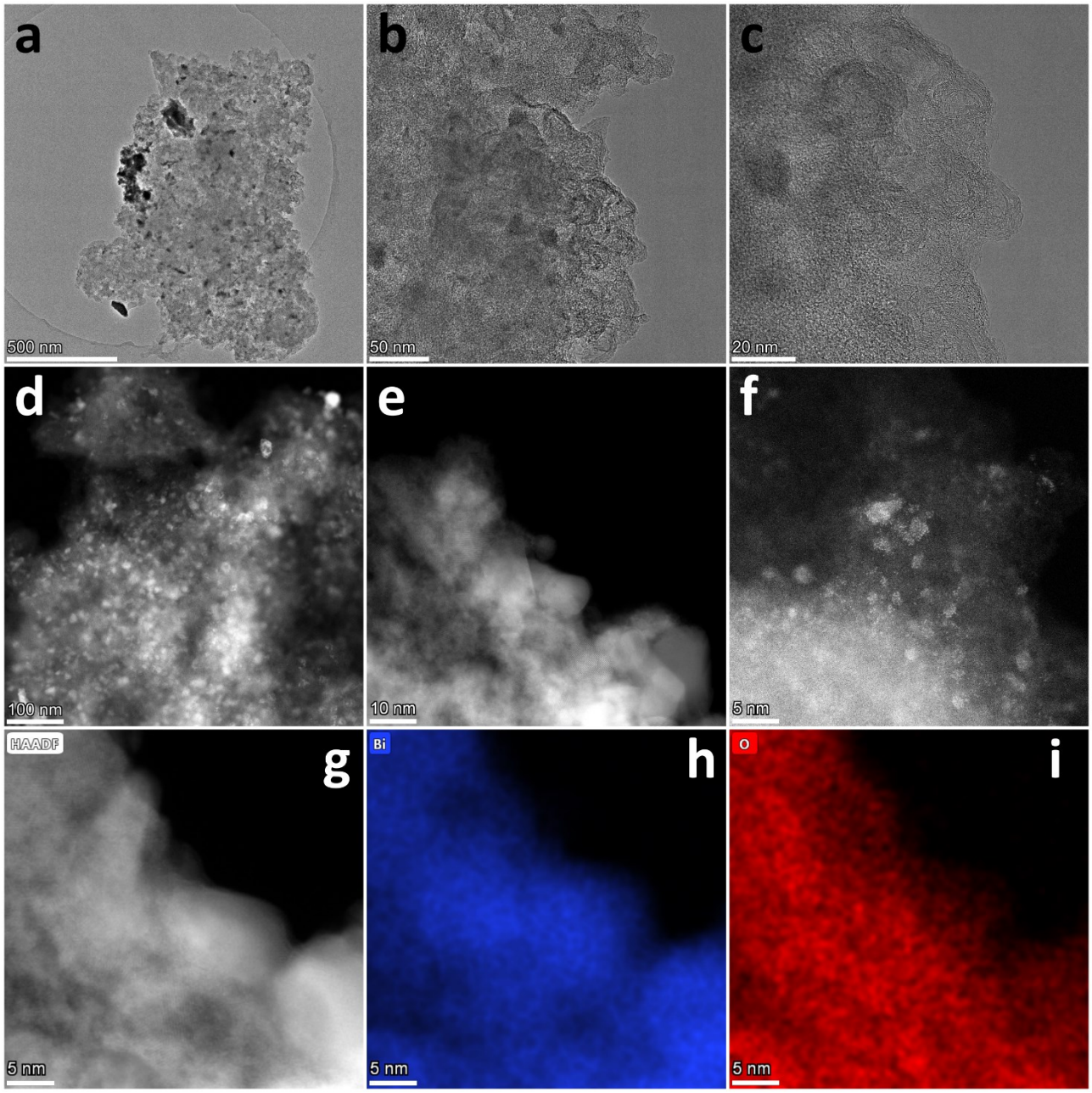

Figure S9: STEM pictures (a, b, c), HAADF TEM pictures (d, e, f) and EDX STEM picture (g, h, i) of BiSub@AC-400 after the stability test.

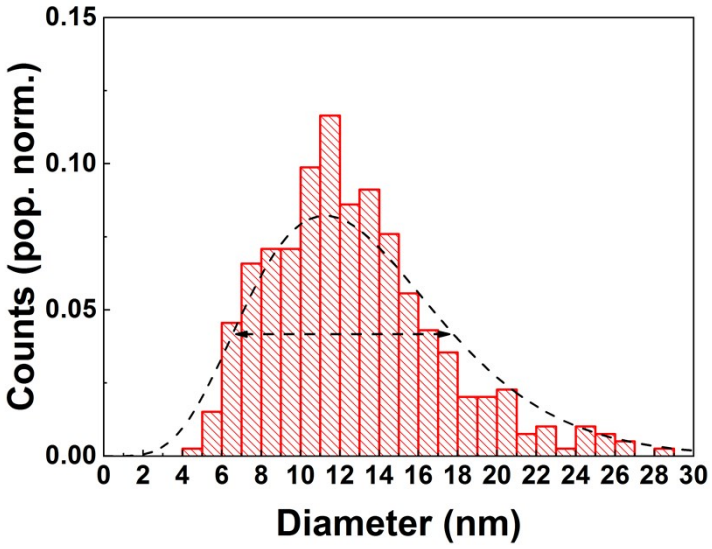

Figure S10: Distribution of the diameters of the bismuth nanoparticles after the stability test.

Bismuth loading effect

The method used to prepare BiSub@AC-400 was employed also for synthesising two additional electrocatalysts with a different BiSub loading, i.e. half or double than what employed in the synthesis of BiSub@AC-400 (Tab. S5). The resulting electrocatalysts were tested in the reduction of CO_2 to formate in CO_2-saturated 0.5 M $NaHCO_3$ at E = -0.97 V vs RHE (Fig. S11). Activated carbon (AC) without any bismuth supported on it was also tested as electrocatalyst under the same conditions.

Table S5: Bismuth loading and experimental BiSub and AC quantities.

m_{BiSub}/m_{AC} (g/g)	BiSub (g)	AC (g)
0.0 (AC)	none	pure
0.57	0.2930	0.5100
1.15 (BiSub@AC-400)	0.5852	0.5090
2.29	1.1605	0.5070

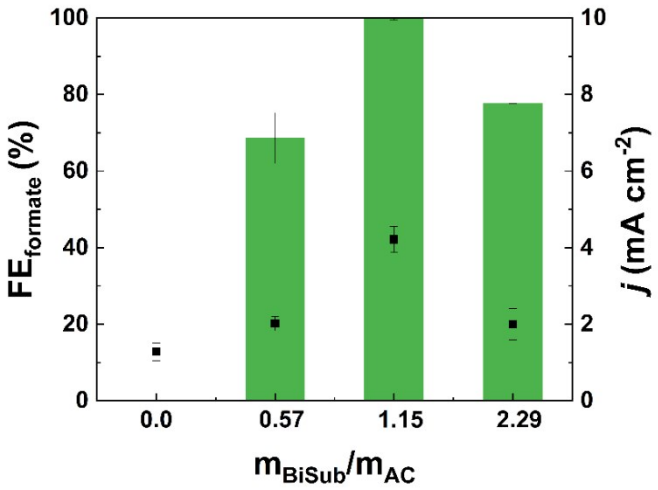

Figure S11: Performance of AC (with no Bi) and of AC-supported Bi-based electrocatalysts synthesised with different BiSub loadings in the reduction of CO_2 to formate in CO_2-saturated 0.5 M $NaHCO_3$ at E = -0.97 V vs RHE [Faradaic efficiency (FE, green bars) and current density (j, black squares)].

Reference electrocatalyst prepared by electrodeposition method

For the preparation of a Bi-electrocatalyst on the AC support by electrodeposition, a 30 mmoL $Bi(NO_3)_3$ in 1 M HNO_3 solution was used as Bi source. The target was to achieve the same Bi-loading as in BiSub@AC-400. For this purpose, the AC was drop-casted on the glassy carbon electrode with the Nafion binder under the same conditions using for the BiSub@AC-400 (*vide supra*). Next, 0.235 mg of Bi were electrodeposited, which was achieved by a charge transfer of 325.5 mC. The electrodeposition was carried at three different potentials: -1.3 V, -1.5 V or -1.7 V vs Ag/AgCl (corresponding to -0.67 V, -0.87 V and -1.07 V vs RHE, respectively). After the deposition, the electrode was gently rinsed with mQ water and used as such.

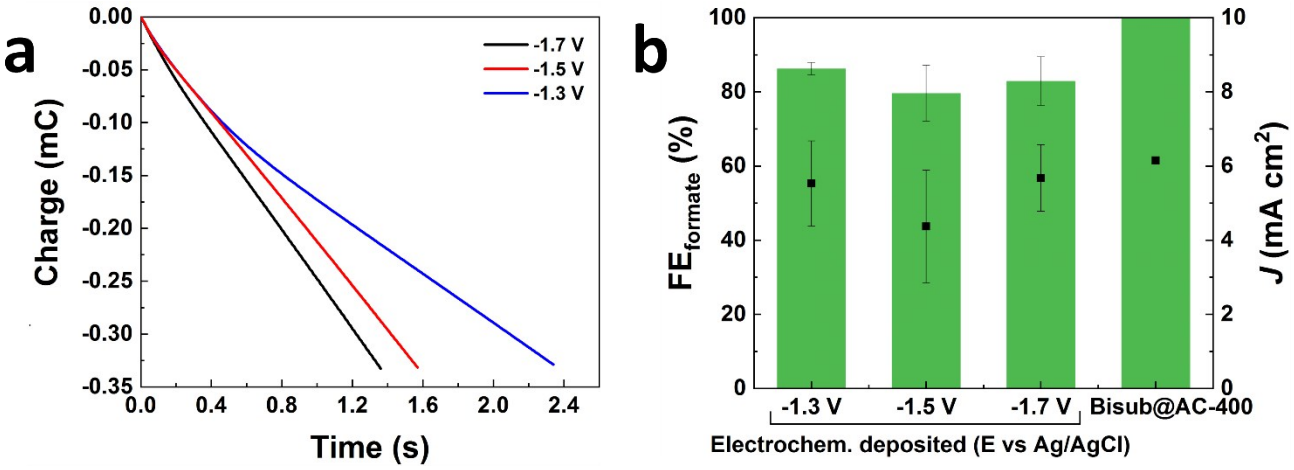

Figure S12: (a) Electrochemical deposition of $Bi(NO_3)_3$ with fixed total charge of 325.5 mC at various deposition potentials. (b) CO_2 electrochemical reduction to formate in CO_2-saturated 0.5M $NaHCO_3$ at E = -1.07 V vs RHE of the three different electrodes produced via electrodeposition and the BiSub@AC-400 catalyst [Faradaic efficiency (FE, green bars) and current density (j, black squares)].

References

1. Y. Zhang, X. Zhang, Y. Ling, F. Li, A. M. Bond and J. Zhang, *Angew. Chem. Int. Ed.*, 2018, **57**, 13283-13287.
2. J. H. Koh, D. H. Won, T. Eom, N.-K. Kim, K. D. Jung, H. Kim, Y. J. Hwang and B. K. Min, *ACS Catal.*, 2017, **7**, 5071-5077.
3. Y. Zhang, F. Li, X. Zhang, T. Williams, C. D. Easton, A. M. Bond and J. Zhang, *J. Mater. Chem. A*, 2018, **6**, 4714-4720.
4. X. Zhang, T. Lei, Y. Liu and J. Qiao, *Appl. Catal. B Environ.*, 2017, **218**, 46-50.
5. W. Lv, J. Bei, R. Zhang, W. Wang, F. Kong, L. Wang and W. Wang, *ACS Omega*, 2017, **2**, 2561-2567.
6. S. Kim, W. J. Dong, S. Gim, W. Sohn, J. Y. Park, C. J. Yoo, H. W. Jang and J.-L. Lee, *Nano Energy*, 2017, **39**, 44-52.
7. H. Yang, N. Han, J. Deng, J. Wu, Y. Wang, Y. Hu, P. Ding, Y. Li, Y. Li and J. Lu, *Adv. Energy Mater.*, 2018, **8**, 1801536.
8. N. Han, Y. Wang, H. Yang, J. Deng, J. Wu, Y. Li and Y. Li, *Nat. Commun.*, 2018, **9**, 1320.
9. Q. Gong, P. Ding, M. Xu, X. Zhu, M. Wang, J. Deng, Q. Ma, N. Han, Y. Zhu, J. Lu, Z. Feng, Y. Li, W. Zhou and Y. Li, *Nat. Commun.*, 2019, **10**, 2807.
10. W. Lv, J. Zhou, J. Bei, R. Zhang, L. Wang, Q. Xu and W. Wang, *Appl. Surf. Sci.*, 2017, **393**, 191-196.
11. D. Zhang, Z. Tao, F. Feng, B. He, W. Zhou, J. Sun, J. Xu, Q. Wang and L. Zhao, *Electrochim. Acta*, 2020, **334**, 135563.
12. Z. Chen, K. Mou, X. Wang and L. Liu, *Angew. Chem. Int. Ed.*, 2018, **57**, 12790-12794.
13. B. Avila-Bolivar, L. Garcia-Cruz, V. Montiel and J. Solla-Gullon, *Molecules*, 2019, **24**.
14. J. Bei, Z. Rui, C. Zhidong, L. Weixin and W. Wei, *Int. J. Electrochem. Sci.*, 2017, **12**, 2365-2375.

15. F. P. G. de Arquer, O. S. Bushuyev, P. De Luna, C. T. Dinh, A. Seifitokaldani, M. I. Saidaminov, C. S. Tan, L. N. Quan, A. Proppe, M. G. Kibria, S. O. Kelley, D. Sinton and E. H. Sargent, *Adv. Mater.*, 2018, **30**, e1802858.
16. P. Deng, H. Wang, R. Qi, J. Zhu, S. Chen, F. Yang, L. Zhou, K. Qi, H. Liu and B. Y. Xia, *ACS Catal.*, 2019, **10**, 743-750.
17. Y. Qiu, J. Du, W. Dong, C. Dai and C. Tao, *J. CO_2 Util.*, 2017, **20**, 328-335.
18. P. Lamagni, M. Miola, J. Catalano, M. S. Hvid, M. A. H. Mamakhel, M. Christensen, M. R. Madsen, H. S. Jeppesen, X. M. Hu, K. Daasbjerg, T. Skrydstrup and N. Lock, *Adv. Funct. Mater.*, 2020, 1910408.
19. F. L. Meng, Q. Zhang, K. H. Liu and X. B. Zhang, *Chemistry*, 2019, **25**.
20. S. He, F. Ni, Y. Ji, L. Wang, Y. Wen, H. Bai, G. Liu, Y. Zhang, Y. Li, B. Zhang and H. Peng, *Angew. Chem. Int. Ed.*, 2018, **57**, 16114-16119.
21. B. Unal, Z. Durmus, H. Kavas, A. Baykal and M. S. Toprak, *Mater. Chem. Phys.*, 2010, **123**, 184-190.
22. T. Hatanpaa, M. Vehkamaki, M. Ritala and M. Leskela, *Dalton T.*, 2010, **39**, 3219-3226.
23. L. Zhang, P. Ghimire, J. Phuriragpitikhon, B. Jiang, A. A. S. Goncalves and M. Jaroniec, *J. Colloid Interf. Sci.*, 2018, **513**, 82-91.
24. M. J. Jabeen Fatima, A. Navaneeth and S. Sindhu, *RSC Adv.*, 2015, **5**, 2504-2510.